© 2017. This manuscript version is made available under the CC-BY-NC-ND 4.0 license http://creativecommons.org/licenses/by-nc-nd/4.0/

Il presente lavoro è stato pubblicato su Carbohydrate Polymers 166(2017) 348–357 con doi: https://doi.org/10.1016/j.carbpol.2017.03.009

Gallium-modified chitosan/poly(acrylic acid) bilayer coatings for improved titanium implant performances

Maria A. Bonifacio,[1] Stefania Cometa,[2§] Manuela Dicarlo,[3§] Federico Baruzzi,[4] Silvia de Candia,[4] Antonio Gloria,[5] Maria M. Giangregorio,[6] Monica Mattioli-Belmonte,[3] Elvira De Giglio[1*]

[1*]Dept. of Chemistry, University of Bari Aldo Moro, Bari, Italy

[2]Jaber Innovation srl, Roma, Italy

[3]Dept. of Clinical and Molecular Sciences, Università Politecnica delle Marche, Ancona, Italy

[4]Institute of Sciences of Food Production (ISPA-CNR), National Research Council of Italy, Bari,

[5]Institute of Polymers, Composites and Biomaterials (IPCB-CNR), National Research Council of Italy, Napoli, Italy

[6]Institute of Nanotechnology (NANOTEC-CNR), National Research Council of Italy, Bari, Italy

[§] *These authors equally contributed to the work.*

* Corresponding author. Tel/Fax: +39 080 5442021.

E-mail address: elvira.degiglio@uniba.it (E. De Giglio)

Abstract

A gallium-modified chitosan/poly(acrylic acid) bilayer was obtained by electrochemical techniques on titanium to reduce orthopaedic and/or dental implants failure. The bilayer *in vitro* antibacterial properties and biocompatibility were evaluated against *Escherichia coli* and *Pseudomonas aeruginosa* and on MG63 osteoblast-like cells, respectively. Gallium loading into the bilayer was carefully tuned by the electrochemical deposition time to ensure the best balance between antibacterial activity and cytocompatibility. The 30 minutes deposition time was able to reduce *in vitro* the viable cell counts of *E. coli* and *P. aeruginosa* of 2 and 3 log cfu/sheet, respectively. Our results evidenced that the developed antibacterial coating did not considerably alter the mechanical flexural properties of titanium substrates and, in addition, influenced positively MG63 adhesion and proliferation. Therefore, the gallium-modified chitosan/poly(acrylic acid) bilayer can be exploited as a promising titanium coating to limit bacterial adhesion and proliferation, while maintaining osseointegrative potential.

Keywords: Chitosan-based Bilayer, Gallium, Titanium, Antibacterial agents, Electrochemical deposition, Biocompatibility.

Chemical compounds studied in this article

Chitosan hydrochloride (PubChem SID: 295370713); gallium (III) nitrate hydrate (PubChem CID: 11550823); poly(acrylic acid) (PubChem CID: 6581); titanium (PubChem CID: 23963); ammonium peroxydisulfate (PubChem CID: 62648).

1. Introduction

Large bone defects are not a rare issue to deal with, and when high load-bearing implants are required, Titanium (Ti) and its alloys represent the gold standard. Among the noteworthy features of Ti, there is the match between lightweight and desirable Young's modulus, as well as the durability given by corrosion resistance (Rack & Qazi, 2006). Since the implant surface is in direct contact with the surrounding tissues, several strategies have been promoted in order to enhance Ti implants biocompatibility (Sidambe, 2014) and, among these, the development of bioactive polymeric coatings represents one of the most effective approaches.

Microbial colonization and biofilm formation are among the major causes of orthopaedic and/or dental titanium-based implants failure (Hedrick et al., 2006). The local antimicrobial delivery represents a well-experimented smart strategy to hinder bacterial adhesion and proliferation, avoiding the side effects arising from a massive systemic antibiotic administration (Trampuz et al., 2003). In this respect, the implant coating could be also designed in order to perform a main role in infection prevention.

Gallium (Ga) has shown bacteriostatic activity and efficacy in the treatment of several disorders associated with bone resorption, including Paget's disease and cancer-related hypercalcemia (Bernstein, 1998; Bernstein, 2013). Furthermore, it potentiates the antimicrobial action of lactoferrin (Berlutti et al., 2008) and stops bone resorption by quenching osteoclasts activity (Verron et al., 2010). Moreover, gallium has recently shown efficacy in infections treatment: exploiting the chemical similarity with Fe^{3+}, Ga^{3+} can interfere with iron metabolism of a wide range of bacteria (Kelson et al., 2013).

Poly(acrylic acid) (PAA), is stable, non-toxic, non-inflammatory and able to mimic bone-surrounding tissues. PAA coatings, synthesized on Ti or its alloys via an electrochemical process, have been previously studied, highlighting both biocompatible and anticorrosion performances for metallic implants (De Giglio et al., 2007). In this work, poly(acrylic acid) has the role to promote the adhesion of a gallium-modified chitosan layer on titanium.

Chitosan (CS) is a biopolymer that shows biocompatible, biodegradable, osteoconductive, and wound healing properties (Muzzarelli et al. 2009), thanks to its structural and chemical homology to proteoglycans found in the extracellular matrix. For all these reasons and also thanks to its ability to complex metal ions (Varma et al., 2004), it was selected as vehicle to deliver the metallic antibacterial agent to the local implant-tissue interface.

In this work, a two-step electrochemical procedure was used to develop on titanium a polymeric bilayer, obtained by electropolymerization of a PAA layer followed by electrochemical deposition of CS-Ga layer, with the double aim of preventing infections and enhancing implant biocompatibility.

An accurate physico-chemical, morphological and mechanical characterizations of PAA/CS-Ga bilayer were reported. Antibacterial performances against *E. coli* and *P. aeruginosa* were evaluated, as well as compatibility with MG63 human osteoblast-like cells.

2. Materials and methods

2.1 Materials

All reagents purchased from commercial sources were used as provided unless otherwise stated. Acrylic acid (AA), used as monomer, ammonium peroxydisulfate ($(NH_4)_2S_2O_8$), used as electrochemical initiator, and gallium nitrate ($Ga(NO_3)_3$), used as source of gallium ions, were purchased from Sigma Aldrich® (Milan, Italy). Chitosan hydrochloride (deacetylation degree 86.4%, viscosity 4 mPa·s, approx. molecular weight 30-400kDa, according to manufacturer) was obtained from HEPPE MEDICAL CHITOSAN GmbH (Germany). Titanium sheet electrodes were mechanically polished by fine diamond paper and then by Al_2O_3 powder (50 μm). After this treatment, before polymer deposition, each electrode (2 cm^2) was cleaned by an ultrasonic bath using ethanol and successively triple-distilled water. All microbiological media and supplements were purchased from Biolife Italiana srl (Milan, Italy). The materials used to determine the gallium

amount loaded and released by the coating using DPASV were reported in the Supplementary data (S1.1 Paragraph).

2.2 Bilayer electrosynthesis

All electrochemical experiments were carried out using a PAR VersaSTAT4 potentiostat-galvanostat (Princeton Applied Research, Hampshire, UK) and a three-electrode cell. A titanium sheet was used as cathodic working electrode, while a platinum wire was the anodic one.
All potentials were related to the reference system used: Ag/AgCl (KCl sat.) in water (0.197V vs SHE at 25°C). PAA coatings were prepared directly on titanium by cyclic voltammetry in aqueous solution of acrylic acid (AA) 0.1M and ($(NH_4)_2S_2O_8$) 0.1M (experimental parameters: initial potential 0.0V; final potential -1.2V; scan rate 100mV/s; 20 cycles) (De Giglio et al., 2007). Successively, CS and Ga ions were electrodeposited on the coating by chronoamperometry (-1.5V). Three different deposition times (15, 30 and 60 minutes) were used to obtain the CS-Ga layer over PAA. The dried samples were sterilized by UV treatment before *in vitro* antibacterial and cytocompatibility tests.

2.3 Gallium quantification and release

The gallium amount loaded in or released by the bilayer was evaluated, after acid digestion, by differential pulse anodic stripping voltammetry (DPASV). The same technique was previously used by other authors to determine gallium traces (Udisti & Piccardi, 1988). However, in this work the electrolytic composition of the sample solution and the instrumental settings were carefully modified in order to optimize the measurement conditions.
Gallium release evaluation was performed, under stirring, dipping coated titanium sheets in 1mL of PBS (pH 7.4) at 37°C for 12, 24, 48, 72, 120 and 168 h. After the incubation time, the PBS was subjected to acid digestion and the gallium released quantified by DPASV.

The acid digestion was carried out according to a previously reported procedure (Danielsson et al., 1981). The digested samples were then cooled at room temperature and diluted with distilled water to a final volume of 25 mL. All gallium measurements were performed on a 757VA Computrace voltammetric analyzer (Metrohm srl, Origgio, VA, Italy). Details on the cell setup, calibration and measurements were reported in the Supplementary data (S1.1. Paragraph).

2.4 Physico-chemical, morphological and mechanical characterization

2.4.1 Fourier Transform Infrared Spectroscopy in Attenuated Total Reflection mode (FT-IR/ATR)

FT-IR/ATR analysis was performed on a Spectrum Two PE instrument using the Universal ATR accessory (Single Reflection Diamond) (PerkinElmer Inc, Waltham, MA) at 4 cm^{-1} resolution. The samples were analysed without any preliminary preparative step.

2.4.2 X-ray Photoelectron Spectroscopy (XPS)

XPS was performed by a Thermo VG Thetaprobe spectrometer (Thermo Fisher Scientific, Inc., Waltham, MA, USA), equipped with a microspot monochromatized AlKα source. Survey scans (binding energy (BE) range 0–1200 eV, FAT mode, pass energy 150 eV) and high-resolution spectra (FAT mode, pass energy 50 eV) were recorded for each sample. Data analysis of the latter was performed using the Avantage software package (version 5.937), which consists of a non-linear least squares fitting program. The experimental points of the detailed spectra were fitted using Gaussian–Lorentzian peaks having the same full width at half maximum (FWHM), according to fitting models applied. Charge referencing was performed by setting the lower binding energy C1s photo-peak (i.e., C1s hydrocarbon peak) at 285.0 eV. Quantification (atomic percentage, At %) was made using normalized peak area. The normalization of the peak area and comparison of data from different element was enabled by correction with empirically derived sensitivity factors according to Scofield libraries (Scofield, 1976) and using the formula already reported (De Giglio et al., 2013).

2.4.3 Atomic Force Microscopy (AFM)

Coating morphology was imaged using atomic force microscopy (AFM) in intermittent contact mode (ICAFM) using an Autoprobe CP-Thermomicroscope. A sharp conical tip with a radius of curvature <10 nm and an amplitude of vibration of 80 kHz (dLever Series Probe) mounted of a p-type doped Si cantilever was used. Atomic force microscopy (AFM) was also used to determine the PAA/CS-Ga thickness. Specifically, PAA/CS-Ga coating was deposited on half of a titanium sheet and by scanning the sample from the PAA/CS-Ga on Ti to the Ti sheet and/or vice versa in different points and using large scan area (90 μm x 90 μm), we measured the step between them. The PAA/CS-Ga thickness was estimated to be 0.6 ± 0.1 μm.

2.4.4 Three-point bending test

The effect of PAA monolayer and PAA/CS-Ga bilayer on the mechanical performance of titanium was assessed by means of three-point bending tests. The specimens (length: 50 mm, width: 10 mm, thickness: 0.5 mm) were tested at a rate of 1 mm/min up to a strain limit of 0.03 mm/mm (3%) using an INSTRON 5566 testing system (INSTRON, Buckinghamshire, UK). The support span-to-depth ratio was 32 to 1. All the tests were carried out in physiological solution at 37.0 ± 0.5°C. Stress and strain (σ and ε, respectively), were evaluated as follows (Equation 1 and 2, respectively):

$$\sigma = \frac{3FL}{2bd^2} \qquad \text{Equation 1}$$

$$\varepsilon = \frac{6Dd}{L^2} \qquad \text{Equation 2}$$

where D is the deflection of the specimen at the middle of the support span, F is the load at a given point of the load-deflection curve, L is the support span, b and d are the sample width and depth, respectively.

2.5 *Bacterial strains, culture conditions and antimicrobial in vitro assays*

The antimicrobial activity of $Ga(NO_3)_3$ and PAA/CS-Ga coatings was evaluated against *Escherichia coli* O157:H7 (avirulent strain) AD615 and *Pseudomonas aeruginosa* DSM 939. The strain DSM 939 was purchased from DSMZ (Braunschweig, Germany) whereas the *E. coli* AD615 was gently provided by ADRIA Développement (Quimper Cedex, France). Both microrganisms were grown as previously described (de Candia, Morea, & Baruzzi, 2015). Details on the antimicrobial *in vitro* assays are reported in the Supplementary data (S1.2 Paragraph).

2.6 Biological Characterization

MG63 human osteoblast-like cells were used for biological characterization of the investigated coatings. Experimental details on cell cultures, MMT viability assay, SEM-EDX analysis, Fluorescence Microscopy, Real-time PCR (RT-qPCR) assay, mRNA expression quantification and Western Blot analysis were reported in the Supplementary data (S1.3 Paragraph).

2.7 Statistical analysis

As far as the antimicrobial test are concerned, the significance of the change in microbial population of each target strains at the beginning of incubation, in PBS at different $Ga(NO_3)_3$ concentrations as well as when target strains were loaded on titanium sheets was calculated with the Friedman test, (Ferguson, 1976). The null hypothesis defined as the absence of effect of the independent variable (incubation conditions) on the dependent variable (viable cell count) was rejected at the level of 5%; then, the nonparametric *post hoc* Mann-Whitney test was applied in order to evaluate statistical differences among microbial populations.

As far as the biological characterization is concerned, results were reported as mean ± standard deviation of three different experiments. Gene expression differences were assessed by one-way ANOVA and Bonferroni's T tests. Statistical significance was tested at $p<0.05$.

GraphPad Prism 4 (GraphPad Software, Inc., CA USA) was used to carry out statistical analysis.

3. Results and discussion

3.1 Bilayer electrosynthesis

Electrochemical polymerization of acrylic acid was carried out by cyclic voltammetry optimizing a previously reported procedure (De Giglio et al., 2007) leading to a thin, strongly adherent PAA coating on titanium substrate. A chronoamperometric deposition of CS in the presence of $Ga(NO_3)_3$ was achieved on a PAA-coated titanium sheet, obtaining a gallium-modified CS upper layer. This strategy was followed since the CS coating failed to adhere directly on bare titanium. Indeed, the presence of the PAA carboxyl groups has been exploited to promote the adhesion of the CS layer on the metallic substrate. On the other hand, the chronoamperometric deposition of gallium ions, in absence of CS, on a previously electrosynthesised PAA layer, produced a coating unsuitable to release gallium ions due to the strong electrostatic interactions between Ga^{3+} and polymer's carboxylate functionalities. Therefore, CS plays a pivotal role interacting with gallium ions, without preventing their release. CS layers, both in presence and absence of $Ga(NO_3)_3$, were deposited onto PAA-coated titanium electrodes by chronoamperometry for three electrodeposition times (15, 30 and 60 minutes). A current decrease was detected during the chronoamperometric step, thus evidencing the CS or CS-Ga deposition on the underlying PAA coating (data not shown).

3.2 Gallium quantification and release

The total gallium amount entrapped in the coatings was estimated by DPASV after an acid digestion. Different experiments, carried out varying the time of the chronoamperometric step, showed that the gallium amount increased with the electrodeposition time. In particular, electrodeposition time equal to 15, 30 and 60 minutes led to total gallium contents of 91 ± 9 μg, 242 ± 3 μg and 611 ± 2 μg, respectively. Therefore, it was possible to modulate the gallium amount in the bilayer, tuning properly the electrodeposition time.

The coatings derived from the three different electrodeposition times showed the following features: the 15 minutes-electrodeposited bilayers showed weak antimicrobial activity, while the 60 minutes-electrodeposited bilayers displayed a cytotoxic behaviour (data not shown). Therefore, our attention was focused only on the 30 minutes-electrodeposited coating since it combined antimicrobial and cell-friendly performances.

In Figure 1, gallium release in PBS over time from the latter coating was reported. The release was characterized by an initial burst, occurred within 24 hours, probably associated to the gallium ions located within the surface CS layer of the specimen. When a plateau was reached, after 48 hours, about 36 µg of gallium ions were released. After 7 days, only the 14.7% of the gallium amount loaded into the coating was released. Indeed, it can be hypothesized that gallium ions, strongly interacting with COO^- groups of the PAA matrix, were probably hindered to be released in the investigated experimental conditions. On the other hand, the amount of gallium released, just after 24 hours, displayed proper antimicrobial performances (see "*In vitro* antibacterial activity" Section).

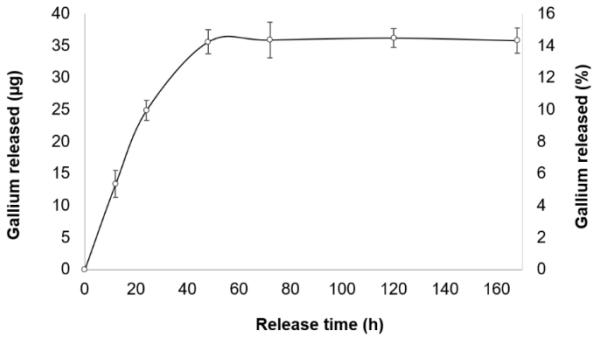

Figure 1: Gallium release from PAA/CS-Ga bilayer over seven days in PBS solution at 37°C.

3.3 Physico-chemical, morphological and mechanical characterization

3.3.1 Fourier Transform Infrared Spectroscopy in Attenuated Total Reflection mode (FT-IR/ATR)

The FT-IR (ATR) spectra of pure PAA coating electropolymerized on Ti and pure CS film drop-casted on Ti, as well as PAA/CS and PAA/CS-Ga bilayers, electrodeposited on Ti as previously described, were shown in Figure 2.

In the PAA spectrum, a broad band due to the stretching of the –OH groups, falling in the range 3100-3600 cm^{-1}, was assigned to the O-H stretching of the hydrogen bonds between OH of COOH groups and/or between adsorbed water molecules. The absorption band at 1703 cm^{-1} was assigned to the C=O stretching vibration from carboxylic groups. Moreover, due to the dissociation of COOH in COO^- groups, two stretching vibrations, $\nu(C=O)_{as}$ and $\nu(C=O)_s$ (asymmetric and symmetric), were observed at 1550 and 1406 cm^{-1}, respectively.

The CS spectrum showed a broad band with two maximum at 3351 and 3290 cm^{-1} assigned to the stretching vibration of O–H and N–H groups associated by intra and intermolecular hydrogen bonding. At 2920 and 2871 cm^{-1} methylene and methyl C-H stretching were detected. Absorption at about 1632 cm^{-1} (amidic C=O stretching) and 1520 cm^{-1} (N–H stretching) were characteristic of amide groups. At 1419 and 1375 cm^{-1} bending vibration of methylene and methyl groups were observed. Finally, absorptions at 1150, 1062 and 1024 cm^{-1} were assigned to CS's saccharide structure (de Vasconcelos et al., 2006).

PAA/CS bilayer spectrum showed absorptions typical of PAA, in addition to absorptions in the range 1180-1020 cm^{-1}, ascribable to the CS structure.

With regard to PAA/CS-Ga bilayer, the $Ga(NO_3)_3$ absorption bands were still evident (in particular, the strong absorption band falling at 1323 cm^{-1} relevant to N-O stretching vibration).

An important feature was that the $\nu(C=O)_{as}$ in PAA/CS bilayer fell at 1548 cm^{-1}, while in PAA/CS-Ga fell at 1584 cm^{-1}, as well as the $\nu(C=O)_s$ in PAA/CS bilayer fell at 1405 cm^{-1}, while in PAA/CS-Ga fell at 1421 cm^{-1}.

The separation between these two $\nu(C=O)$ was higher in the PAA/CS-Ga than in PAA/CS spectrum (i.e., 163 vs. 143 cm^{-1}). In PAA spectrum, this separation was found equal to 144 cm^{-1} (Figure 2).

The higher band separation in PAA/CS-Ga supported the presence of a coordination or a cross-linking between the COO^- groups of PAA and Ga^{3+} ions, as reported in a previous work on Ga-citrate complexes (Clausèn, Öhman, & Persson, 2005). This strong polymer-gallium interaction could explain, as previously argued, the incomplete gallium release evidenced by the DPASV experiments.

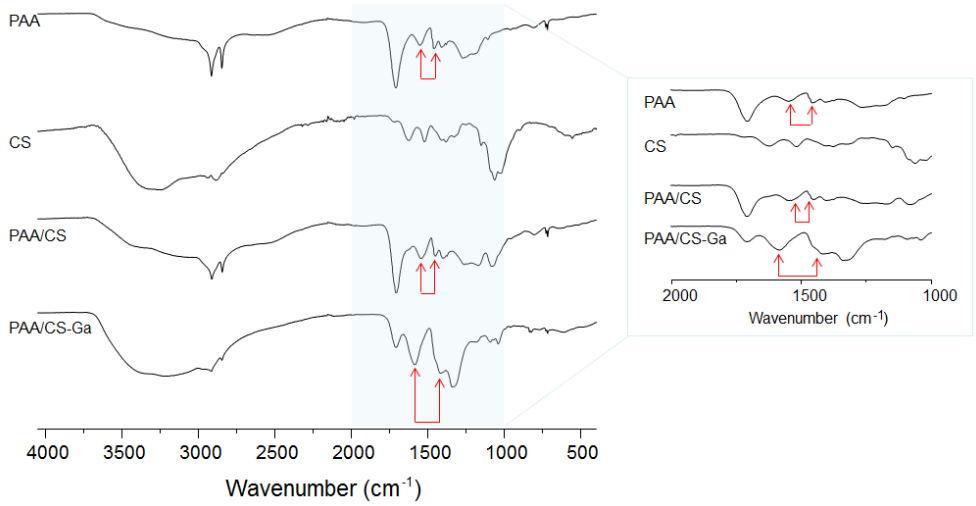

Figure 2: FT-IR (ATR) spectra relevant to PAA, CS (drop-casted on titanium), PAA/CS and PAA/CS-Ga bilayers.

3.3.2 X-ray Photoelectron Spectroscopy (XPS)

XPS investigations were carried out both on PAA/CS bilayer and PAA/CS-Ga coatings, in order to gain information about their surface chemical composition. In PAA/CS bilayer (Figure 3a), signals relevant to oxygen, carbon and nitrogen were detected. In PAA/CS-Ga, a significant gallium Ga2p main signal as well its minor signals were clearly detectable in the wide scan spectrum (Figure 3b). The experimental BEs associated to Ga2p ($Ga2p_{3/2}$= 1118.7 eV) were ascribable to gallium (III) compounds (Cossu et al., 1992). The C1s high-resolution spectrum of PAA/CS and PAA/CS-Ga were also reported in Figure 3c and d, respectively: the relevant attributions and atomic percentages were shown in Figure 3e. Curve fitting of C1s spectra revealed the typical functional groups of both

PAA and CS. Considering that peak D is relevant only to the CS moieties, it is possible to estimate the surface contribution of CS in the C1s signals of the bilayer with and without gallium. Indeed, the (peak D/peak E) ratio in pure CS was estimated to be 6.3, as already reported (Trapani et al., 2011). The same ratio in the PAA/CS bilayer resulted equal to 1.2, while in the PAA/CS-Ga bilayer this ratio was 3.0. These experimental results suggested that, when gallium was added during the second electrodeposition step, the presence of CS on the surface was increased.

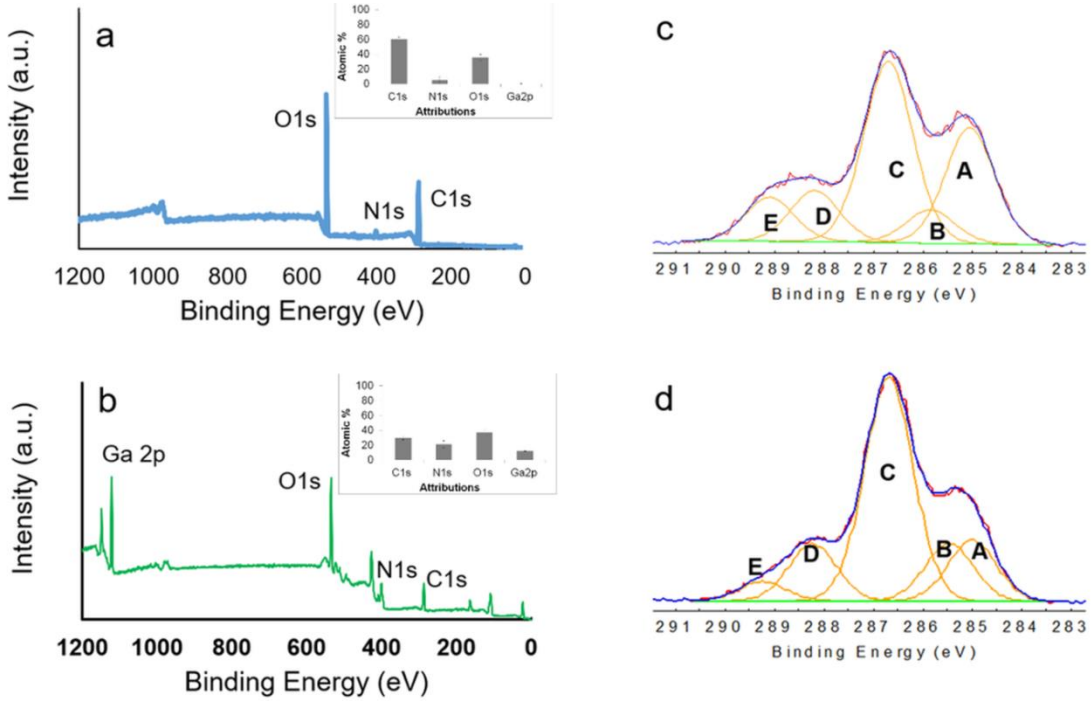

e

Attribution	BE (eV)	At. %	
		PAA/CS	PAA/CS-Ga
A: CH	285.0	27.3	14.7
B: C-N, CH-COOH	285.5	7.9	14.0
C: C–O, C–N^+	286.8	42.5	53.0
D: O-C-O	288.1	12.0	13.7
E: COOH	289.1	10.4	4.6

Figure 3: XPS survey spectra relevant to PAA/CS (a) and PAA/CS-Ga bilayers on Ti (b). In the insets, the atomic percentages of the elements detected on the relevant bilayer surfaces are reported. C1s high-resolution curve fitting of PAA/CS (c) and PAA/CS-Ga bilayers (d), whose peak

attributions, (e) binding energies (BE) and atomic percentages (At. %) relevant to the C1s curve fitting shown in panels (c) and (d). The maximum error on the peak position was ±0.2 eV.

3.3.3 Atomic Force Microscopy (AFM)

Figure 4 compares 40 μm x 40 μm topographical images of (a) Ti sheet, (b) PAA on Ti and (c) PAA/CS-Ga bilayer on Ti. The morphology of the Ti sheet was characterized by parallel features, i.e., grooves and ridges, which can be associated with abrading scratches (Qu et al., 2014; Peláez-Abellán et al., 2012). When PAA was electrosynthesized on Ti, the film texture and surface roughness did not change significantly.

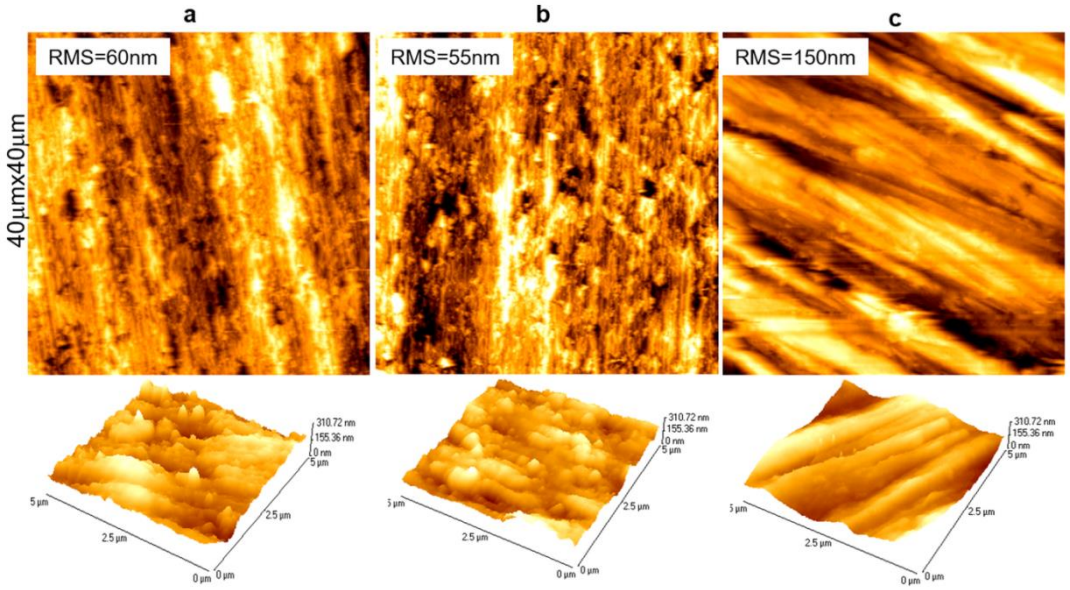

Figure 4: AFM characterization. 40μmx40μm topographical images of (a)Ti electrode, (b) PAA on Ti and (c) PAA/CS-Ga on Ti. Corresponding 3D 5μmx5μm AFM images are also compared at the bottom with the same z-scale 0-310.72 nm.

The fingerprint of the Ti crack structures and submicron heterogeneously-distributed morphology near crack sites were clearly observed on the PAA film. On the contrary, when CS-Ga was electrochemically deposited on PAA (obtaining PAA/CS-Ga bilayer), the morphology strongly changed, resulting in well-oriented bundle formation (Dubey & He, 2012) and in increased

roughness. The bundle formation relevant to PAA/CS-Ga was highlighted by the corresponding 5 μm x 5 μm 3D images shown at the bottom of Figure 4.

3.3.4 Three-point bending test

Results from three-point bending tests on the different kinds of specimens (Ti, Ti/PAA monolayer, Ti/PAA/CS-Ga bilayer) evidenced similar stress-strain curves (Figure 5). An initial linear region of the stress–strain curve was evident. Then, a decrease of the slope was observed up to the strain limit (0.03 mm/mm). Bending modulus (i.e., the slope of the linear region of the curve) and maximum stress were evaluated as mean value ± standard deviation.

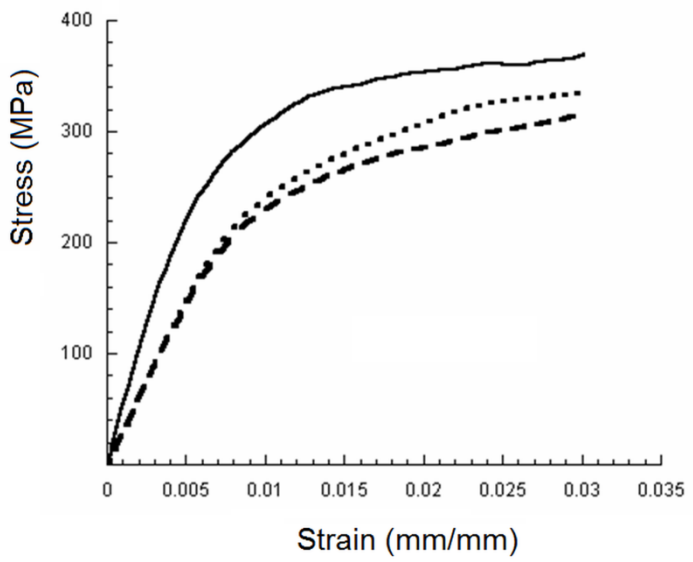

Figure 5: Typical stress-strain curves obtained from three-point bending tests on the different kinds of devices: Ti (full line), Ti/PAA monolayer (dotted line), Ti/PAA/CS-Ga bilayer (dashed line).

Ti samples provided higher values of modulus (58 ± 5 GPa) and maximum stress (370 ± 30 MPa) than those obtained from Ti/PAA monolayer (41 ± 5 GPa and 340 ± 30 MPa) and Ti/PAA/CS-Ga bilayer (40 ± 5 GPa and 310 ± 20 MPa).

It is worth noting that, in the three-point bending test, stress reached the maximum value in the outer regions of the specimen. As a consequence of the polymeric layer, Ti/PAA system provided

values of modulus lower than those obtained from Ti. Even though the support span-to-depth ratio was 32 to 1, taking into account that a shear stress is induced as the bending moment increases linearly from zero at the supports to a maximum value at the central loading point, the three-point bending test may also provide an information on the metal-polymer interface.

In comparison to Ti samples, the results evidenced that the surface coatings did not dramatically alter the maximum flexural stress achieved at 0.03 mm/mm; in addition, the mechanical stability of the coatings (i.e., Ti/PAA monolayer and Ti/PAA/CS-Ga bilayer) can be deduced.

***3.4 In vitro* antibacterial activity**

It is generally accepted that the main biological mechanism of antimicrobial activity of Ga(III) is based on the competition with Fe(III): the gallium-siderophore complexes deregulate several microbial iron-based metabolisms causing cell death (Kelson, Carnevali & Truong-Le, 2013). Differently from Kaneko et al. (2007) who evaluated microbial growth kinetic in 1% TSB supplemented with several $Ga(NO_3)_3$ concentrations, here we assayed antimicrobial activity of $Ga(NO_3)_3$ against two microbial populations in a PBS lacking of carbon, nitrogen sources and other nutrients. As concerns *P. aeruginosa*, Kaneko et al. (2007) demonstrated that strain PA01, inoculated in 1%TSB, was proportionally killed by increasing $Ga(NO_3)_3$ concentration up to 1 mM when it was added during PA01 stationary growth phase. In accordance with this result, our study showed the best killing activity against *P. aeruginosa* DSM 939 (under the stationary growth phase in PBS), increasing $Ga(NO_3)_3$ up to 10 mM (see section S2.1 and Fig. S2).

The antimicrobial activity of the coatings was verified by applying an agar plate method derived from the ASTM E2180 (Standard Test Method for Determining the Activity of Incorporated Antimicrobial Agent(s) in Polymeric or Hydrophilic Materials) as already carried out for zinc oxalate nanoparticles copolymerized with acrylates (Sontakke et al., 2012) and cobalt ferrite nanoparticles (Sanpo et al., 2013).

The application of Friedmann test to viability values of *E. coli* AD615 and *P. aeruginosa* DSM 939 on titanium sheet (before and after incubation), PAA/CS and PAA/CS-Ga coatings, showed that these data did not belong to the same population of values. Then, a pairwise comparison of microbial values from PAA/CS versus PAA/CS-Ga coatings was carried out by applying the Mann-Whitney test. As shown in Figure 6, viability of both target strains decreased (about two log cfu/sheet) significantly in comparison of initial inoculum level (T0) although no differences were found in viable cell count on titanium sheets and PAA/CS coatings. At contrary, viable cell counts of both target strains was reduced significantly ($p < 0.05$) when they were loaded on titanium sheets on which $Ga(NO_3)_3$ was electrodeposited (PAA/CS-Ga coatings). Furthermore, the LIVE/DEAD® BacLight™ assay provided a qualitative evidence of PAA/CS-Ga coatings effectiveness (see Paragraph S2.2 and Fig.S3).

In comparison with $Ga(NO_3)_3$ antimicrobial assays, trials with PAA/CS-Ga coatings produced a better result. In absence of direct evidences, it is possible to hypothesize that PAA/CS-Ga coatings released a higher amount of Ga(III) than that occurring in $Ga(NO_3)_3$ solutions, due to the precipitation of large part of Ga(III) as $Ga(OH)_3$ when the $Ga(NO_3)_3$ was dispersed in buffer with pH range between pH 3 and 9 (Rzhepishevska et al., 2011). On the other hand, an additional antimicrobial effect of gallium retained in the coatings could not be excluded. Moreover, the reduced mobility of microbial cells into the agar matrix, as happens in microbial biofilms, could be a further reason of the increased antimicrobial efficacy of gallium ions, that were demonstrated to inhibit biofilm formation in *in vitro* assays (Kaneko et al., 2007).

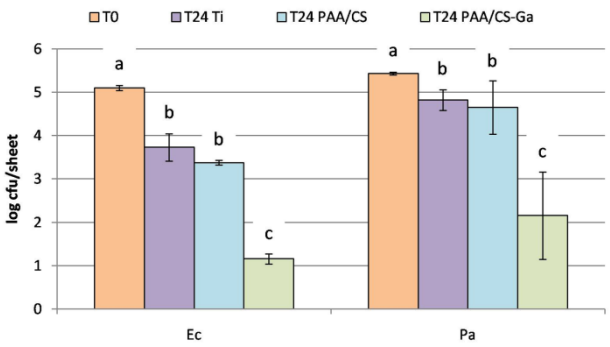

Figure 6: Antimicrobial activity. Viable cell count of Escherichia coli O157:H7 AD615 (Ec) and Pseudomonas aeruginosa DSM 939 (Pa) before incubation (T0) and after 24 h at 37°C loaded onto titanium sheets (T24 Ti), PAA/CS (T24 PAA/CS) and PAA/CS-Ga bilayers (T24 PAA/CS-Ga). The data were consolidated from three independent experiments; bars represent mean values ± standard deviation. The same letter represents values statistically similar ($p > 0.05$) within the same strain.

3.5 Biological evaluation

Considering the role of osteoblastic cells in the bone remodelling process, we investigated whether the PAA/CS-Ga coating could affect osteoblastic behaviour in terms of viability, proliferation and relevant osteoblastic markers. We used the osteoblastic cell line MG63 (Billiau et al., 1977), which is a well-known osteosarcoma cell line commonly used as osteoblastic model to test titanium implants (Martin et al., 1995; De Giglio et al., 2010). Tests were performed at two different time points: 2 days (T1) was chosen to evaluate the effect of the burst release of gallium, whilst 7 days (T2) was selected to test its effect at a longer time.

Viability on PAA/CS and PAA/CS-Ga coatings was investigated by MTT assay: no significant differences were detected between MG63 cultured on tissue culture plates (TCPs) and those seeded on bare Ti at both time points analysed (Figure 7a). At T1 a significant reduction in cell viability in comparison with controls was detected for both Ti coatings (i.e., PAA/CS and PAA/CS-Ga), even if with values higher than 65%. This reduction could be at least in part due to a different

adhesion/proliferation of cells between chitosan and plastic surfaces. Comparing absorbance data obtained from cells cultured on the two different Ti coatings, it can be argued that the observed reduction in cell viability was not ascribable to gallium doping. No significant differences were detectable in all samples at T2.

Cytoskeletal detection was performed at T1 in order to ascertain the initial cell adhesion to the substrates, since this event is crucial in implant osseointegration (Mattioli-Belmonte et al., 2014). Actin fluorescence images of MG63 (Figure 7b) showed well spread cells on all analysed samples, with a preserved organization of the cytoskeletal structures that determines the global cell shape. SEM observations followed the same trend of MTT results: at T1, a higher cell colonization was detected on bare Ti in comparison with the two tested coatings, whilst at T2 cells distribution was almost homogeneous onto all analysed surfaces, with a typical spindle-shaped morphology (Pautke et al., 2004) (Figure 7c). Interestingly, cell orientation on PAA/CS-Ga coating was superimposable to surface bundles detected with AFM, suggesting that the changes in topography could represent an instructive pattern for cell arrangement. Moreover, EDX mapping (Figure 7d) evidenced the distribution of Ti, Ca, P and Ga on the different cultured surfaces and confirmed that the presence of gallium did not affect cell adhesion and spreading.

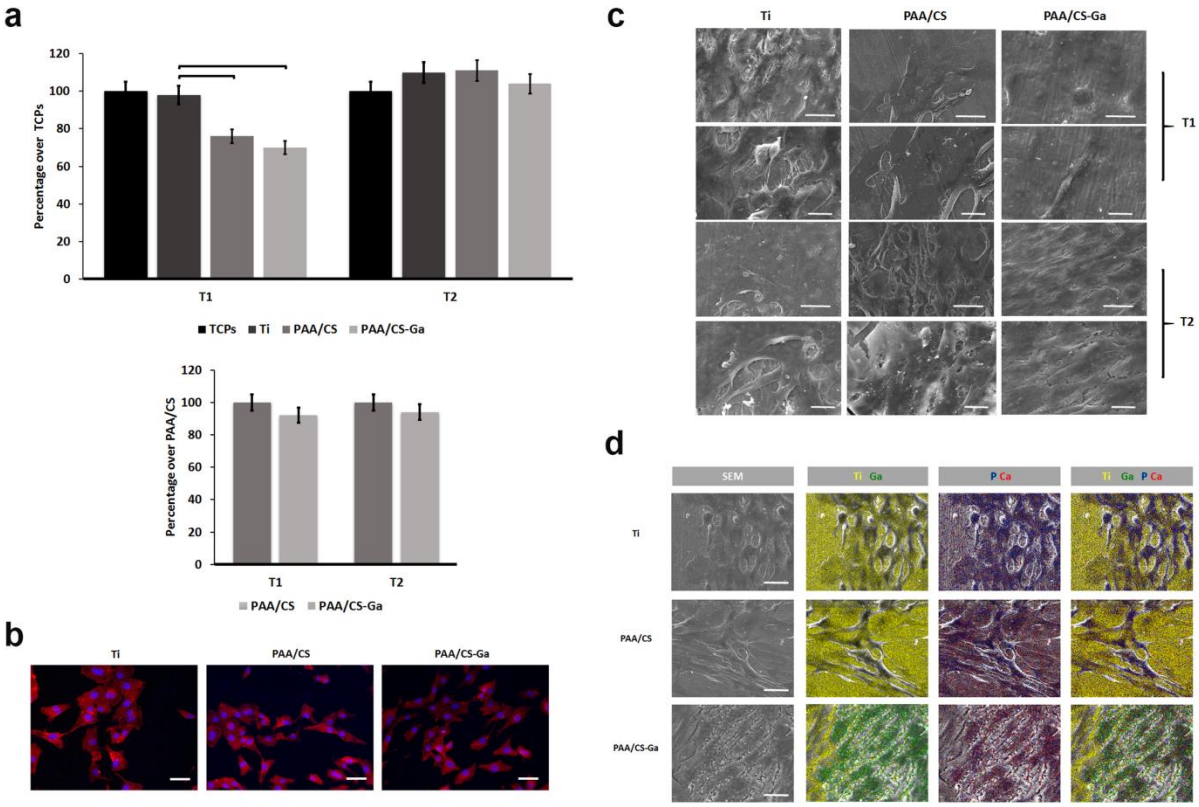

417 **Figure 7:** Cell adhesion and viability: a) MTT viability test of MG63 cultured for 2 (T1) and 7
418 (T2) days on Tissue Culture plates (TCPs), bare Titanium (Ti), PAA/CS and PAA/CS-Ga bilayers.
419 Data are expressed as percentage of TCPs control culture or of PAA/CS, Mean values ± SD are
420 reported; brackets indicate statistic significant ($p < 0.05$) differences; b) Fluorescence microscopy
421 images of actin filament (red) distribution in cell cultured on Ti, PAA/CS and PAA/CS-Ga, nuclei
422 are stained in blue (scale bars 10 µm); c) Scanning electron micrographs of cells (asterisks) cultured
423 on Ti, PAA/CS and PAA/CS-Ga at both time point analysed (scale bars 20 µm); d) EDX mapping
424 of element distribution (Ti=yellow; Ga=green; P=blue, Ca=red) in cell cultures at T2 (scale bars 20
425 µm).
426
427 To evaluate whether the proposed coatings (i.e. PAA/CS and PAA/CS-Ga bilayers) may affect
428 MG63 behaviour, mRNA expression of genes involved in bone growth was evaluated. Analysis of
429 their relative expression ($2^{-\Delta ct}$) evidenced a reduction in mRNA between cells seeded on TCPs and

those seeded on the two coatings; these differences were significantly marked for runx2, collagen type I and ALP (Figure 8a).

In order to better elucidate if these changes were attributable to gallium doping, we analysed mRNA fold regulation ($2^{-\Delta\Delta ct}$) in comparison to control cultures (TCPs).

a

	TCPs		PAA/CS		PAA/CS-Ga	
	MEAN	DS	MEAN	DS	MEAN	DS
Runx2	1.06E-02	9.24E-04	4.18E-03	4.65E-04	6.61E-03	3.93E-04
Bmp2	4.25E-03	2.44E-03	3.65E-03	8.24E-04	5.63E-03	1.90E-03
Coll Type I	8.92E-02	3.36E-02	4.92E-02	8.60E-04	4.74E-03	2.74E-05
ALP	3.14E-02	1.62E-03	5.13E-03	1.96E-04	7.22E-03	7.09E-04
Sparc	8.22E-01	2.82E-02	7.09E-01	1.51E-02	6.39E-01	4.18E-02

Bmp2=bone morphogenetic protein 2; Runx2=runt-related transcription factor 2; ALP= Alkaline Phosphatase; Sparc= osteonectin.

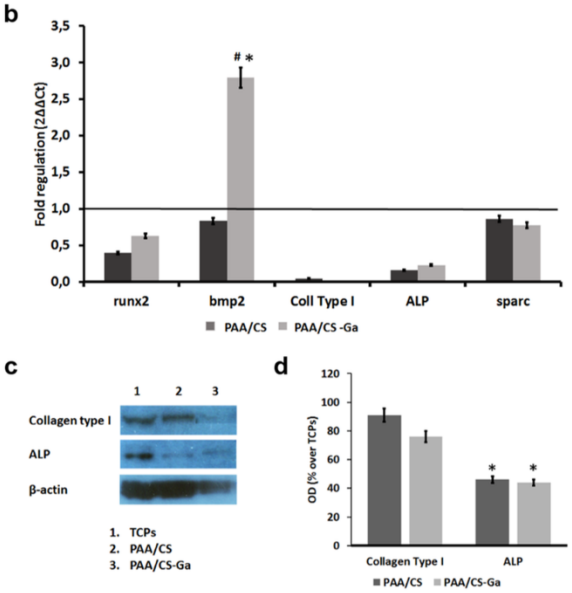

Figure 8: MG63 gene and protein expression: a) mRNA relative expression; b) Histogram depict changes in mRNA expression in MG63 cultured for 7 days (T2) days on PAA/CS and PAA/CS-Ga bilayers. Data are expressed as Fold-regulation (2^-ΔΔCt) (see S1.3 Paragraph). The black line indicates the range of physiological mRNA expression changes;*p<0.05 vs TCPs; # p<0.05 vs PAA/CS; c) Western blot analysis of Collagen Type I and Alkaline Phosphatase (ALP) protein content in MG63 cultured on TCPs, PAA/CS and PAA/CS-Ga bilayers; d) Densitometric quantitation of the blots presented in c. Results are expressed as percentage of control cells (TCPs); *p<0.05 vs TCPs.

This analysis suggested that gallium did not produce negative effect on osteoblastic marker expression, on the contrary it appeared to enhance (2.5 fold) bmp2 mRNA expression (Figure 8b). As far as Collagen Type I and ALP are concerned, qRT-PCR showed a significant reduction in their mRNA expression in comparison with the controls; at contrary, coatings unaffected osteonectin (sparc) expression. Western Blot analysis detected an unchanged expression of Collagen Type I protein content between the coatings and control cultures and a significant reduction of ALP on both the tested coatings respect to TCPs (Figures 8c and d). However, no significant differences related to the presence of gallium were observed. The detected decrease in ALP production on the gallium-modified coating is in contrast with recent literature (Cochis et al., 2016; Verron et al., 2010). This evidence could be, at least in part, related to the different pattern of expression of MG63 in comparison with other human (i.e. Saos2) or murine (i.e. MC3T3E-1) osteoblastic cell lines at the analysed time point (Pautke et al., 2004). On the contrary, the positive effect of gallium is appreciable in our system by the detection of the upregulation of bmp2, which is a genetic marker of the early osteoblastic differentiation. Overall, biological data are consistent with the lack of adverse effects of the proposed coatings up to 7 days.

4. Conclusions

A novel gallium-modified coating on titanium implants has been proposed to the aim of preventing microbial colonization without affecting osseointegration. The investigated PAA/CS-Ga bilayer was obtained on titanium substrates by low-cost electrochemical techniques. Since gallium exerts its antibacterial activity by “mimicking” Fe(III), the application of PAA/CS-Ga coatings releasing Ga(III) ions could produce an antimicrobial effect, in particular when microbial cells start to adhere to inert surfaces, as happens during first stage of biofilm formation. In addition, viability and proliferation of MG63 osteoblast-like cells were unaffected by the presence of gallium in the PAA/CS-Ga bilayer: among several genetic marker evaluated, gallium upregulated bmp2, a genetic marker of early osteoblastic differentiation. Biological data of PAA/CS-Ga bilayer on osteoblast-

like cell lines and bacterial pathogens strengthen its effectiveness for a potential application of this coating in orthopaedic and/or dental field.

Acknowledgments

This work was supported by Università degli Studi di Bari Aldo Moro. The authors greatly acknowledge Mr. Domenico Benedetti for his unique expertise and valuable technical support in DPASV measurements.

References

Berlutti, F., Superti, F., Nicoletti, M., Morea, C., Frioni, A., Ammendolia, M. G., Battistoni A., Valenti, P. (2008) Bovine lactoferrin inhibits the efficiency of invasion of respiratory A549 cells of different iron-regulated morphological forms of Pseudomonas aeruginosa and Burkholderia cenocepacia. *International journal of immunopathology and pharmacology*, 21(1), 51-59.

Bernstein, L. R., (1998) Mechanisms of therapeutic activity for gallium. *Pharmacological reviews*, 50(4), 665-682.

Bernstein, L. R. (2013) Gallium, therapeutic effects. In Kretsinger, R.H.; Uversky, V.N.; Permyakov, E.A, *Encyclopedia of Metalloproteins* (pp. 823-835) Springer New York.

Billiau, A., Edy, V. G., Heremans, H., Van Damme, J., Desmyter, J., Georgiades, J. A., & De Somer, P. (1977). Human interferon: mass production in a newly established cell line, MG-63. *Antimicrobial agents and chemotherapy*, 12(1), 11-15.

Clausén, M., Öhman, L. O., & Persson, P. (2005). Spectroscopic studies of aqueous gallium (III) and aluminum (III) citrate complexes. *Journal of inorganic biochemistry*, 99(3), 716-726.

Cochis, A., Azzimonti, B., Della Valle, C., De Giglio, E., Bloise, N., Visai, L., ... & Chiesa, R. (2016). The effect of silver or gallium doped titanium against the multidrug resistant Acinetobacter baumannii. *Biomaterials*, 80, 80-95.

Cossu, G., Ingo, G. M., Mattogno, G., Padeletti, G., & Proietti, G. M. (1992). XPS investigation on vacuum thermal desorption of UV/ozone treated GaAs (100) surfaces. *Applied surface science*, 56, 81-88.

Danielsson, L. G., Jagner, D., Josefson, M., Westerlund, S. (1981) Computerized potentiometric stripping analysis for the determination of cadmium, lead, copper and zinc in biological materials. *Analytica Chimica Acta*, 127, 147-156.

De Candia, S., Morea, M., & Baruzzi, F. (2015). Eradication of high viable loads of Listeria monocytogenes contaminating food-contact surfaces. *Frontiers in microbiology*, 6, art. n. 733.

De Giglio, E., Cometa, S., Cioffi, N., Torsi, L., Sabbatini, L. (2007) Analytical investigations of poly (acrylic acid) coatings electrodeposited on titanium-based implants: a versatile approach to biocompatibility enhancement. *Analytical and bioanalytical chemistry*, 389(7-8), 2055-2063.

De Giglio, E., Cometa, S., Ricci, M. A., Zizzi, A., Cafagna, D., Manzotti, S., ... & Mattioli-Belmonte, M. (2010). Development and characterization of rhVEGF-loaded poly (HEMA–MOEP) coatings electrosynthesized on titanium to enhance bone mineralization and angiogenesis. *Acta biomaterialia*, 6(1), 282-290.

De Giglio, E., Cafagna, D., Cometa, S., Allegretta, A., Pedico, A., Giannossa, L. C., Sabbatini, L., Mattioli-Belmonte, M., Iatta, R. (2013) An innovative, easily fabricated, silver nanoparticle-based titanium implant coating: development and analytical characterization. *Analytical and bioanalytical chemistry*, 405(2-3), 805-816.

de Vasconcelos, C. L., Bezerril, D. P., Dos Santos, D. E. S., Dantas, D. T., Pereira, M. R., Fonseca, J. L. C. (2006) Effect of molecular weight and ionic strength on the formation of polyelectrolyte complexes based on poly (methacrylic acid) and chitosan. *Biomacromolecules*, 7(4), 1245-1252.

Ferguson G. A. (1976). *Statistical Analysis in Psychology and Education* (4th ed.). New York: McGraw-Hill.

Hedrick, T. L., Adams, J. D., Sawyer, R. G. (2006) Implant-associated infections: an overview. *Journal of long-term effects of medical implants*, 16(1) 83-99.

Dubey, M., & He, H. (2012). *Morphological and Photovoltaic Studies of TiO_2 NTs for High Efficiency Solar Cells*. INTECH Open Access Publisher.

Kaneko, Y., Thoendel, M., Olakanmi, O., Britigan, B. E., & Singh, P. K. (2007). The transition metal gallium disrupts Pseudomonas aeruginosa iron metabolism and has antimicrobial and antibiofilm activity. *The Journal of clinical investigation*, 117(4), 877-888.

Kelson, A. B., Carnevali, M., & Truong-Le, V. (2013). Gallium-based anti-infectives: targeting microbial iron-uptake mechanisms. *Current opinion in pharmacology*, 13(5), 707-716.

Martin, J. Y., Schwartz, Z., Hummert, T. W., Schraub, D. M., Simpson, J., Lankford, J., ... & Boyan, B. D. (1995). Effect of titanium surface roughness on proliferation, differentiation, and protein synthesis of human osteoblast-like cells (MG63). *Journal of biomedical materials research*, 29(3), 389-401.

Mattioli-Belmonte, M., Cometa, S., Ferretti, C., Iatta, R., Trapani, A., Ceci, E., ... & De Giglio, E. (2014). Characterization and cytocompatibility of an antibiotic/chitosan/cyclodextrins nanocoating on titanium implants. *Carbohydrate polymers*, 110, 173-182.

Muzzarelli, R. A. A. (2009) Chitins and chitosans for the repair of wounded skin, nerve, cartilage and bone. *Carbohydrate polymers*, 76(2), 167-182.

Pautke, C., Schieker, M., Tischer, T., Kolk, A., Neth, P., Mutschler, W., & Milz, S. (2004). Characterization of osteosarcoma cell lines MG-63, Saos-2 and U-2 OS in comparison to human osteoblasts. *Anticancer research*, 24(6), 3743-3748.

Peláez-Abellán, E., Duarte, L. T., Biaggio, S. R., Rocha-Filho, R. C., & Bocchi, N. (2012). Modification of the titanium oxide morphology and composition by a combined chemical-electrochemical treatment on cp Ti. *Materials Research*, 15(1), 159-165.

Qu, Q., Wang, L., Chen, Y., Li, L., He, Y., & Ding, Z. (2014). Corrosion Behavior of Titanium in Artificial Saliva by Lactic Acid. *Materials*, 7(8), 5528-5542.

546 Rack, H. J., & Qazi, J. I. (2006). Titanium alloys for biomedical applications. Materials
547 Science and *Engineering: C*, 26(8), 1269-1277.
548 Rzhepishevska, O., Ekstrand-Hammarström, B., Popp, M., Björn, E., Bucht, A., Sjöstedt, A.,
549 ... & Ramstedt, M. (2011). The antibacterial activity of Ga3+ is influenced by ligand complexation
550 as well as the bacterial carbon source. *Antimicrobial agents and chemotherapy*, *55*(12), 5568-5580.
551 Sanpo, N., Berndt, C. C., Wen, C., & Wang, J. (2013). Transition metal-substituted cobalt
552 ferrite nanoparticles for biomedical applications. *Acta biomaterialia*, *9*(3), 5830-5837.
553 Scofield, J. H. (1976) Hartree-Slater subshell photoionization cross-sections at 1254 and
554 1487 eV. *Journal of Electron Spectroscopy and Related Phenomena*, 8(2), 129-137.
555 Sidambe, A. T. (2014). Biocompatibility of advanced manufactured titanium implants—A review.
556 *Materials*, 7(12), 8168-8188.
557 Sontakke, T. K., Jagtap, R. N., Singh, A., & Kothari, D. C. (2012). Nano ZnO grafted on
558 MAA/BA/MMA copolymer: An additive for hygienic coating. *Progress in Organic Coatings*,
559 74(3), 582-588.
560 Trampuz, A., Osmon, D. R., Hanssen, A. D., Steckelberg, J. M., Patel, R. (2003) Molecular
561 and antibiofilm approaches to prosthetic joint infection. *Clinical orthopaedics and related research*,
562 414, 69-88.
563 Trapani, A., De Giglio, E., Cafagna, D., Denora, N., Agrimi, G., Cassano, T., Gaetani, S.,
564 Cuomo, V., Trapani, G. (2011) Characterization and evaluation of chitosan nanoparticles for
565 dopamine brain delivery. *International journal of pharmaceutics*, 419(1), 296-307.
566 Udisti, R., & Piccardi, G. (1988). Determination of gallium traces by differential pulse
567 anodic stripping voltammetry. *Fresenius' Zeitschrift für analytische Chemie*, 331(1), 35-38.
568 Varma, A. J., Deshpande, S. V., & Kennedy, J. F. (2004). Metal complexation by chitosan
569 and its derivatives: a review. *Carbohydrate Polymers*, 55(1), 77-93.

570 Verron, E., Masson, M., Khoshniat, S., Duplomb, L., Wittrant, Y., Baud'huin, M., Badran,
571 Z., Bujoli, B., Janvier, P., Scimeca, J. C., Bouler, J. M., Guicheux, J., (2010) Gallium modulates
572 osteoclastic bone resorption *in vitro* without affecting osteoblasts. *Br J Pharmacol*. 159(8):1681-92.